Fucoidan- and Ciprofloxacin-Doped Plasma-Activated Polymer Coatings on Biodegradable Zinc: Hemocompatibility and Drug Release

Radka Gorejová, Kadir Ozaltin, Ivana Šišoláková,* Miriam Kupková, Petr Sáha, and Renáta Oriňaková
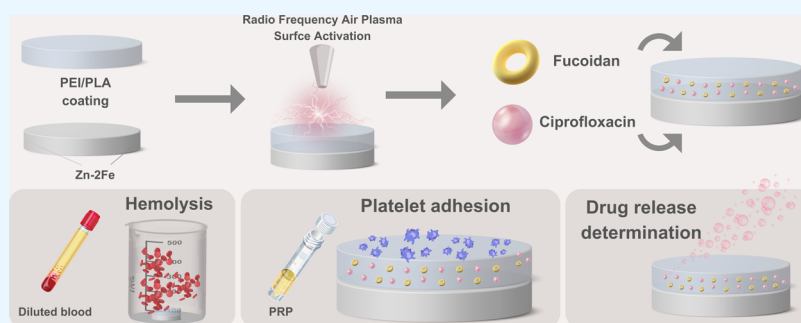
Read Online

ACCESS | Metrics & More | Article Recommendations | Supporting Information

ABSTRACT: Blood-contacting medical devices such as biodegradable metallic bone implant materials are expected to show excellent hemocompatibility both *in vitro* and *in vivo*. Different approaches are being studied and used to modify biomaterial surfaces for enhanced biocompatibility and hemocompatibility. However, the composition of degradable biomaterial must address several drawbacks at once. Iron-reinforced zinc material was used as a metallic substrate with improved mechanical properties when compared with those of pure zinc. Poly(lactic) acid (PLA) or polyethylenimine (PEI) was selected as a polymeric matrix for further doping with antibiotic ciprofloxacin (CPR) and marine-sourced polysaccharide fucoidan (FU), which are known for their antibacterial and potential anticoagulant properties, respectively. Radiofrequency air plasma was employed to induce metallic/polymer-coated surface activation before further modification with FU/CPR. Sample surface morphology and composition were studied and evaluated (contact angle measurements, AFM, SEM, and FT-IR) along with the hemolysis ratio and platelet adhesion test. Successful doping of the polymer layer by FU/CRP was confirmed. While PEI induced severe hemolysis over 12%, the PLA-coated samples exhibited even lower hemolysis (~2%) than uncoated samples while the uncoated samples showed the lowest platelet adhesion. Moreover, gradual antibiotic release from PLA determined by the electrochemical methods using screen-printed carbon electrodes was observed after 24, 48, and 72 h, making the PLA-coated zinc-based material an attractive candidate for biodegradable material design.

1. INTRODUCTION

Materials originating from natural or synthetic sources that are developed for use in medical applications to interact with biological systems and replace, repair, or enhance their function are called biomaterials.[1−5] Common types of biomaterials are prepared from metals, ceramics, polymers, and composites.[5−7] A new group of materials, biodegradable metals (BMs), that are designed to degrade *in vivo* over a selected time is currently being developed.[8−11] BMs are materials that are supposed to degrade by natural biological processes to substances that are well tolerated by the host environment. These materials must be made from biocompatible elemental metals such as magnesium, iron, and zinc, and their alloys or composites.[12−16] Among them, zinc is considered to be the most promising due to its beneficial health effects connected to bone healing, wide processing possibilities due to the low melting point, and tunable

corrosion rate.[17] Degradable metallic implants can complement the frequently used inert metallic materials and be useful in specific applications in which the presence of the implant in the body over a long time is unnecessary. This will eliminate the need for a second surgery to remove the implant after fulfilling its mission, which reduces the risk of implant rejection and even provides the release of beneficial substances participating in the bone tissue regeneration process (e.g., zinc ions).[18] During the development of any material intended

for implantation in the body, its complete biological compatibility with the host environment must be ensured.

Degradable implants, as blood-contacting devices, interact with blood in several ways. Released degradation products may cause the alteration of the blood pH or a change in the ion concentration of the blood. Moreover, they may also induce oxidative stress or platelet activation and aggregation. Therefore, the hemocompatibility of BMs is of huge importance to consider in biomaterial design and development. Several studies have found that the release of their degradation products can lead to changes in blood clotting and platelet aggregation properties.[19−25] To improve the hemocompatibility of BMs, researchers have proposed various surface modifications (e.g., polymeric coatings or surface functionalization), to reduce the adverse effects of degradation products on blood.[26−30] Additionally, alteration in the material bulk composition (e.g., use of alloying elements or fabrication of composite materials) can also improve the biocompatibility and, moreover, the mechanical properties of these metals.[31−33] For such a reason, zinc−iron alloy was selected as a matrix material in our study, with improved mechanical properties when compared with pure zinc. To further improve the biological properties of the proposed Zn−Fe material, surface activation and coating with polymers were performed.

Coating with a polymeric thin layer is one of the frequent scientific approaches employed to modify the surface of metallic implants.[34−38] Two polymers were selected for the Zn−Fe matrix modification, namely, poly(lactic) acid (PLA) and polyethylenimine (PEI). PLA coatings have been previously used to improve the biocompatibility and corrosion resistance of metallic biomaterials[39,40] by decreasing the pace of the metal ions released into the adjacent tissues. Despite the many biological benefits of zinc, too high of a concentration of zinc ions can cause a local toxic effect, which can be prevented by reducing the rate of its degradation, for example, by applying a polymer coating. Moreover, the degradation product of PLA (lactic acid) is nontoxic and can be metabolized and eliminated by the body.[41] Polyethylenimine (PEI) is a cationic polymer that has been shown to promote cell adhesion and proliferation and has been used in various biomedical applications[42−45] as a coating or gene carrier. PEI coatings have also been used as a surface modification for BMs in our previous work to improve their biocompatibility and mechanical properties and to influence corrosion properties.[46] Though, cytotoxicity of PEI has been a concern recently, which highlights the importance of optimizing the properties and concentration of the coating material to ensure its biocompatibility.

To prevent postoperation infection at the site of the implantation, antibiotic agents are being introduced to biodegradable coatings of metallic biomaterials.[47−49] Ciprofloxacin (CPR), used in our study, is a broad-spectrum antibiotic belonging to the fluoroquinolone class of antibiotics commonly used to treat various bacterial infections.[50] The optimal concentration of ciprofloxacin in a polymeric coating of a biomaterial should be sufficient to provide effective antimicrobial activity while minimizing any potential cytotoxic or hemolytic effects. Several studies investigated the use of ciprofloxacin as an additive therapeutical agent at concentrations ranging from 1 to 50 mM.[51−53] Esrafilzadeh et al.[51] studied the cytotoxic effect of CPR and found that concentrations ≤125 μg/mL demonstrated no toxicity against B35 neuroblastoma cells while values over 250 μg/mL showed

toxicity. Therefore, there is a need to study and determine the concentration of a released drug during the coating and BMs dissolution, which was done using electrochemical methods in our study.

For further targeted enhancement of the material hemocompatibility, the marine-sourced polysaccharide fucoidan (FU) has been chosen for use. Fucoidan is a natural polysaccharide that is found in various species of brown seaweed, and it has shown *in vitro* anticoagulant properties.[54,55] The involvement of sulfate groups in the FU structure is acclaimed to contribute to its anticoagulant activity by interacting with blood coagulation factors. Studies have shown that fucoidan can inhibit blood clot formation by affecting various steps in the coagulation cascade, such as the activation of thrombin inhibitors.[55] Fucoidan has been shown to have anti-inflammatory and antioxidant properties as well.[55,56] However, further studies are still needed to understand the operation mechanisms and potential undesirable effects of FU, along with its optimal dosing and form of utilization.

Our study aimed to prepare and characterize a new biodegradable material with a functionalized (PEI/PLA coated, doped with ciprofloxacin and fucoidan) surface as a potential anticoagulant drug-releasing platform for biodegradable implant material fabrication. The Fe−Zn metallic matrix was used due to the promising properties of zinc as a new biodegradable metal, which was reinforced with 2 wt % iron to enhance its mechanical performance. PLA and PEI were used as CPR and FU carriers that can also prevent the corrosion of zinc that is too rapid and therefore lower its potential toxic effects. In addition, rapid electrochemical detection of released ciprofloxacin was performed by using screen-printed carbon electrodes.

2. MATERIALS AND METHODS

2.1. Zinc-Based Substrate Preparation. Zinc (Zn) (99.9% purity, Centralchem, Slovakia) and iron (Fe) (99.5% purity, Alfa Aesar, Germany) powders were used as raw materials for sample preparation. Powders were mechanically mixed before the compression. Two grams of the mixture were cold-pressed to form green compacts in the form of pellets with a diameter of 12 mm and height of 4 mm with a composition of 98 wt % zinc +2 wt % iron (labeled as Zn-2Fe). The composition of the experimental sample was chosen based on a previous study,[23] in which the effect of iron content on mechanical properties and hemocompatibility was studied, while the material containing 2 wt % iron was evaluated as most suitable for further use. Compacts were heated from room temperature to 330 °C, held at 330 °C for 60 min using a high-temperature furnace (Nabertherm RHTC 80-230/15, Lilienthal, Germany), and spontaneously cooled to room temperature. The sintering occurred under an inert atmosphere (Argon, 5.0 purity, flow rate of 4 L min^{-1}). Sintered samples were ground with three different grits (#320, #600, #1200), ultrasonically cleaned in absolute ethanol for 10 min, and dried at 60 °C for 1 h.

2.2. Metallic Surface Plasma Activation. Radiofrequency (RF) air plasma (50 W reactor power and 13.56 MHz frequency) generated by a plasma reactor (PICO, Diener, Germany) was used for 60 s to activate a metallic sample surface before coating application. The plasma treatment method was used to enhance the chemical interactions of metals with active groups of the coating

materials and to enhance the surface roughness before coating application. Air was used with a 20 standard cubic centimeters per minute flow rate as a discharge gas under a chamber pressure of 50 Pa.

2.3. Coatings Preparation. Polyethylenimine (PEI, 60–100 kDa, 50 wt % in H_2O, Sigma-Aldrich, Germany) and poly(lactic acid) (PLA, 2003D, NatureWorks) coating solutions were prepared for material surface modification, and a sol–gel method was used to coat the metallic Zn-2Fe samples. PEI solution was further diluted to 10 wt % with absolute ethanol. PLA coating solution was prepared by dissolving PLA in dichloromethane (DCM) at 500 rpm for 1 h to obtain a 2.5 wt % concentration. Immediately after the plasma treatment, samples were placed into 24 well plates and immersed in 0.6 mL of PEI (10 wt/v% ethanol solution) or PLA (2.5 wt/v% dichloromethane solution) for 90 min and then left to dry overnight at 37 °C. RF plasma was applied for the second time after the PEI/PLA coating deposition under the conditions described above.

2.4. Drug Loading. Fucoidan (from *Fucus vesiculosus*, Sigma-Aldrich, Germany) and ciprofloxacin (≥98% (HPLC), Sigma-Aldrich, Germany) were used in this study. The doping of the polymer PEI/PLA layer with CPR-loaded fucoidan (0.1 wt % CPR) was performed from aqueous fucoidan solution (1 wt %, pH = 5) to enhance the anticoagulant and antibacterial properties of the material. The CPR-loaded fucoidan solution (0.6 mL) was applied onto the surface of the Zn-2Fe-PLA and Zn-2Fe-PEI samples for 90 min, and then removed and dried at 37 °C overnight. The composition and the design of the prepared samples are summarized in Table 1.

Table 1. Sample Types Used during the Experiments[a]

sample denotation	metallic substrate	first layer of coating	second layer of coating
Zn-2Fe	Zn-2Fe		
Zn-2Fe-PEI-FU/CPR	Zn-2Fe	PEI (10 wt %)	FU/CPR (1 wt %/0.1 wt %)
Zn-2Fe-PLA-FU/CPR	Zn-2Fe	PLA (2.5 wt %)	FU/CPR (1 wt %/0.1 wt %)

[a]PEI - polyethyleneimine, PLA - poly(lactic) acid, FU - fucoidan, CPR - ciprofloxacin.

2.4.1. UV–vis Spectroscopy for CPR Incorporation Efficiency Determination. UV–vis spectroscopy method was used to determine the amount of ciprofloxacin loaded into the polymer coating. Coated samples were prepared as described above. The polymer-coated sample was immersed in 10 mL of a suitable solvent (dichloromethane for the PLA coating, ethanol solution for the PEI coating). Once the PLA/PEI coating was dissolved, the solution was filtered to remove any insoluble residues or impurities. The absorbance of the sample was measured using a UV–vis spectrophotometer (Biochrom WPA Lightwave II, Biochrom Ltd., UK), and the concentration of ciprofloxacin was calculated using the Beer–Lambert law. Loading efficiency (LE) was calculated according to eq 1:

$$LE\ (\%) = 100 \times \frac{\text{non-incorporated CPR}}{\text{initial CPR}} \quad (1)$$

2.5. Sample Surface Morphology and Chemical Composition. Scanning electron microscopy (SEM) coupled with energy-dispersive X-ray spectroscopy (EDX) (JEOL JSM-7000F, with EDX INCA, Tokyo, Japan) was used for the surface morphology and chemical composition investigation of bare and coated samples.

Atomic force microscopy (AFM) was used to study the surface topology of the sample using a Dimension Icon (Bruker, Karlsruhe, Germany) microscope. All experiments were performed by peak force tapping mode using a ScanAsyst-Air Si/Nitride probe (Bruker, Santa Barbara) with $k = 0.4$ N m^{-1} of the spring constant value of the cantilever. A scanning area of 1×1 μm for each sample was investigated with a frequency of 1 Hz. Average surface roughness (R_a) values were analyzed using the NanoScope Analysis software.

Samples were molded in PolyFast, sanded with four different grit sandpapers (#320, #600, #1200), polished with diamond paste (1 μm) on satin polishing cloth moistened with kerosene, washed, and rinsed with alcohol for microstructure analysis. For microstructure analysis, an optical microscopy technique was used (Olympus CX71 inverted metallographic microscope with an Olympus DP12 camera, Tokyo, Japan) in polarized light and differential interference contrast mode. The samples were ultrasonically cleaned in methanol before observation. The microstructure was disclosed after etching in a 0.5% aqueous NaOH solution.

IRTracer-100 infrared spectrometer (Shimadzu, Japan) was used to record the FT-IR spectra using the attenuated total reflection (ATR) method.

2.6. Contact Angle Measurements and Surface Energy Evaluation. Contact angles were measured for the metallic surface energy evaluation using two liquids (water and diiodomethane). The detailed testing procedure can be found in the Supporting Information.

2.7. Blood Tests. Hemolysis induced by the tested material and platelet morphology as an *in vitro* thrombosis parameter was studied. The hemocompatibility tests were performed in triplicates and under ISO 10993-4: Selection of Tests for Interactions with Blood[56] norm and in compliance with the Declaration of Helsinki. The detailed testing procedure can be found in the Supporting Information.

2.8. Cyclic Voltammetry for CPR Release Determination. To determine the amount of ciprofloxacin released after 24, 48, and 72 h in PBS, cyclic voltammetry as a simple and accurate method was used. Since the aim of the antibiotic component is to serve as an immediate postoperation treatment, a short-time release profile was studied in our case. All voltammetric measurements were performed using potentiostat/galvanostat Autolab PGSTAT 302N (Metrohm, Switzerland) and realized by potential scanning between +0.2 and +1.2 V at a scan rate of 100 mV/s. Screen-printed carbon electrodes (SPCEs) of type 110Ni (NiNPs/SPCE, Metrohm, Switzerland) were used for all electrochemical measurements. NiNPs/SPCEs are made of the carbon electrode, Ag/AgCl electrode, and NiNPs-modified carbon electrode as the counter, reference, and working electrode, respectively. The limit of detection (LOD) was also calculated. All electrochemical experiments were carried out at atmospheric pressure and laboratory temperature in the phosphate-buffered saline solution (PBS) simulating human body conditions.

3. RESULTS

3.1. Metallic Sample Surface Morphology and Wettability. Metallic materials composed of zinc and 2 wt % iron were prepared via a powder metallurgical route. Samples in the form of cylindrical pellets were sintered in a high-temperature furnace and were further examined. SEM was
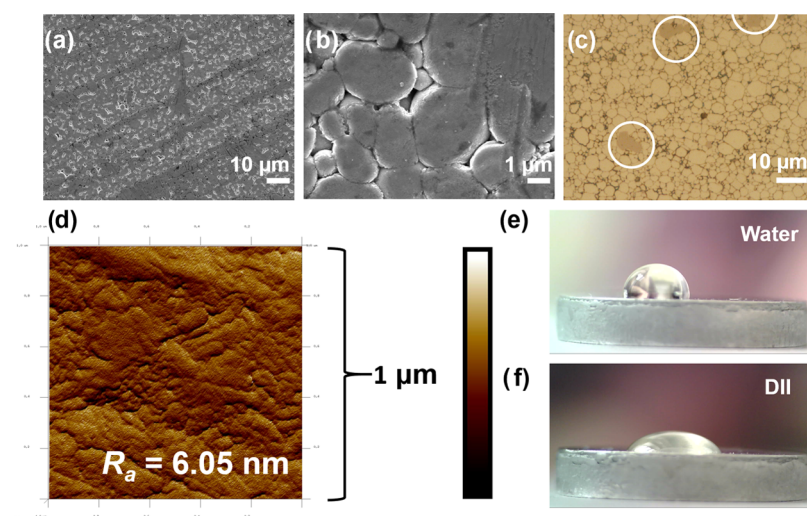
Figure 1. (a, b) SEM micrographs of the uncoated Zn-2Fe sample. (c) Optical micrographs of uncoated Zn-2Fe sample surface with iron particles highlighted in white/with arrows. (d) A detailed topography of the Zn-2Fe material obtained from the AFM measurements. (e) Water and (f) diiodomethane contact angles for Zn-2Fe polished surfaces.

employed for the study of sample surface morphology (Figure 1a,b). The appearance of a sample surface after polishing with different grits resulted in a textured, smoother surface. The surface became increasingly flatter and more polished as finer grits (up to #1200) were used. The powder metallurgy preparation resulted in the formation of globular, soft-edged grains due to the consolidation of small metallic particles (Figure 1b). Globular zinc particles in a size ranging from 1 to 10 μm and rather irregular Fe-based clusters were found in the material microstructure (Figure 1c). Since the low sintering temperature was chosen (330 °C), no intermetallic phases occurred in the material; however, zinc diffusion into the iron particles is anticipated.

AFM was used to study the surface morphology of sintered samples at the nanoscale level (Figure 1d). The average roughness value was obtained from the AFM measurements to illustrate the texture/topography of a material. The value of R_a = 6.05 nm was obtained for the Zn-2Fe sample and can be considered low, indicating a relatively smooth material.

Water and diiodomethane contact angles were measured to evaluate the hydrophobicity or hydrophilicity of the prepared surface (Figure 1e,f). The obtained values are summarized in Table 2. The surface tension of the uncoated sample was also determined (Table 2).

Table 2. Surface Tension of the Uncoated Zn-2Fe Sample Calculated from Contact Angle Measurements Using Water and Diiodomethane

sample	contact angle (deg)		γ_s (mN m^{-1})
Zn-2Fe	water	diiodomethane	19.89
	94.09 ± 1.33	52.65 ± 1.88	

3.2. Coating Deposition and Characterization. EDX was used to study the elemental composition of the polymer-coated materials. Figure 2 depicts SEM micrographs of the prepared sample surfaces along with the corresponding EDX spectra. Zinc, iron, and oxygen were detected for the uncoated Zn−Fe surface (Figure 2b) reflecting the chemical composition of initial powders used to prepare the alloy. Zinc and iron

oxides were created during the sample and powders handling on air.

In the case of Zn-2Fe-PEI-FU/CPR, carbon, zinc, oxygen, and sulfur were detected (Figure 2d). The presence of carbon can be attributed to both the polymer and the FU/CPR presence in the coating. Sulfur detected in the spectrum originating from the fucoidan sulfate groups confirmed its successful deposition. However, several prominent cracks appeared in a PEI layer after the application of the second layer (Figure 2c) due to the higher solubility in water when compared with PLA leading to layer disruption. According to this, zinc and oxygen originating from the metallic substrate were also present in the EDX spectrum, indicating lower thickness of PEI coating.

Only carbon, oxygen, and sulfur were detected at the surface of the PLA-based coating (Figure 2f) suggesting homogeneous coating distribution and sufficient thickness (which can be further optimized by the dip-coating process repetition), which was also confirmed by SEM (Figure 2e).

EDX provides information about the elemental composition of the coating but does not provide information about the chemical structure. Therefore, FT-IR, which provides more detailed information about the chemical bonds and functional groups present in the coating material, was employed to study the coated surface. Figure 3 shows the FT-IR spectra of all of the studied materials, along with the representation of chemical structures used in the coating (Figure 3a).

An uncoated Zn-2Fe sample was used as a reference material (Figure 3d). An absorption band in the range 500−470 cm^{-1} was found, which is characteristic of the Zn−O stretching vibration. The band at 885 cm^{-1} belongs to the stretching vibration of Zn−OH. Both zinc oxide and hydroxide originate from metallic surface oxidation. The C−H (carbon−hydrogen) symmetric and asymmetric stretching vibrations were observed at 1056 cm^{-1} and 2980−2900 cm^{-1}.

The spectra changed significantly, and a large number of bands were observed after coating. For the Zn-2Fe-PEI-FU/CPR (Figure 3c), characteristic N−H (nitrogen−hydrogen) stretching vibration was observed at around 3400 cm^{-1} and C−N stretch at 1220 cm^{-1} originating from PEI. In the spectrum of Zn-2Fe-PLA-FU/CPR (Figure 3d), carbonyl
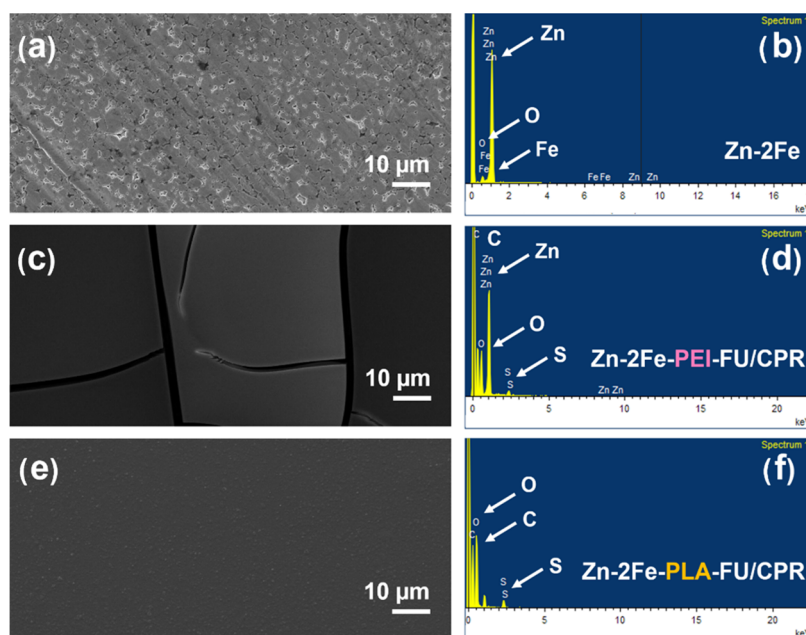
Figure 2. SEM micrographs with corresponding EDX analyses: (a, b) Zn-2Fe; (c, d) Zn-2Fe-PEI-FU/CPR; (e, f) Zn-2Fe-PLA-FU/CPR.
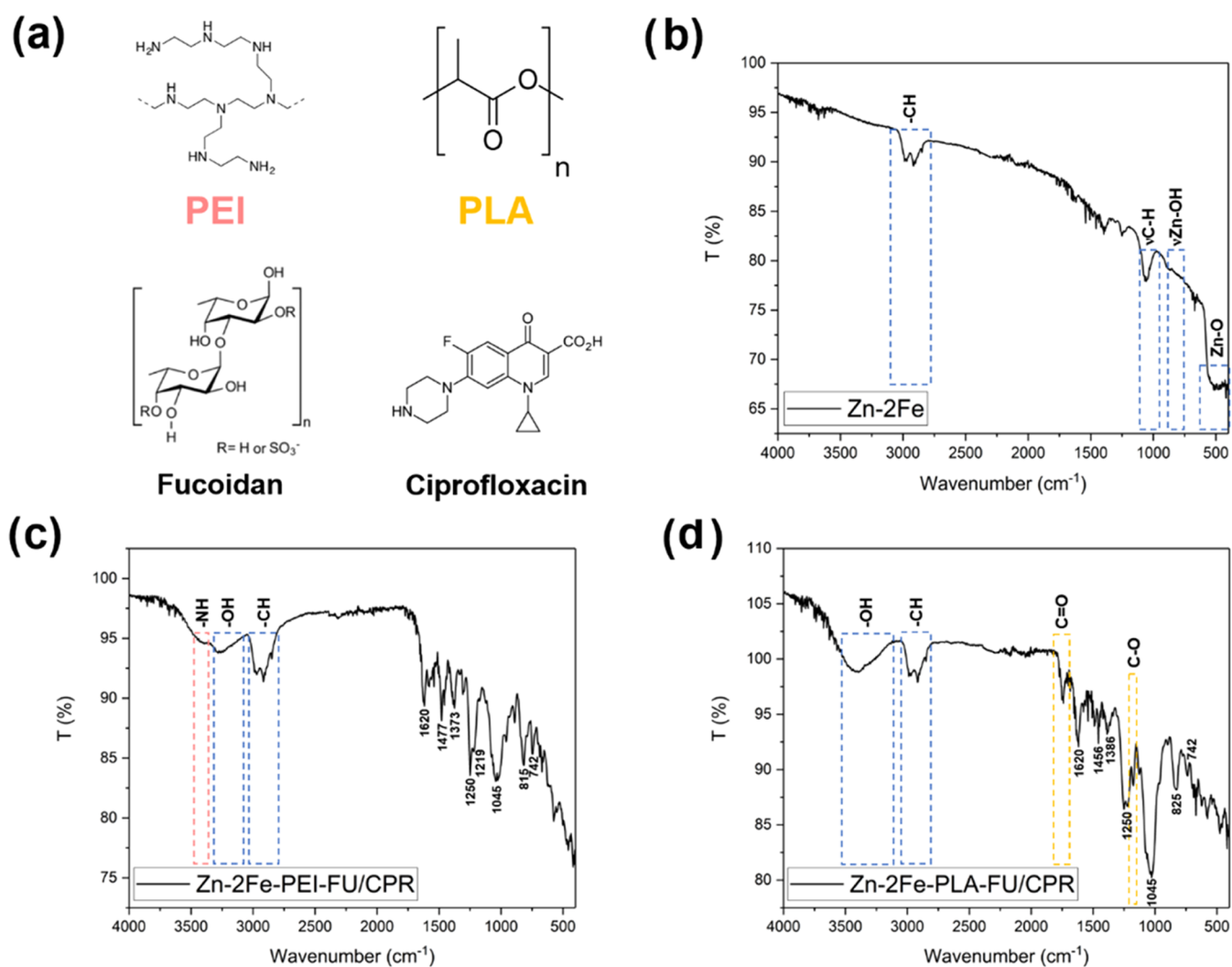

Figure 3. (a) Chemical structure of chemicals used in the coating preparation. FT-IR spectra of (b) uncoated Zn-2Fe reference sample; (c) Zn-2Fe-PEI-FU/CPR; (d) Zn-2Fe-PLA-FU/CPR.

(C=O) stretching vibration occurred at 1740 cm$^{-1,}$ and the band for the vibration of the carbon−oxygen bond at 1460 and 1180 cm^{-1} emerged from the PLA.

Bands originating from fucoidan and ciprofloxacin, respectively, were observed in both spectra of the coated samples. The O−H band referring to the vibrational mode of the hydroxyl (OH) group in molecules with stretching frequency was found at 3550−3100 cm^{-1}. The C=C stretching vibrations in the quinoline ring appeared at 1620 cm^{-1} in both (PEI and PLA) cases. Besides that, the C=C bond from an aromatic compound (benzene) was detected at 1370−1380 cm^{-1}. Typical bands characteristic of fucoidan were found at 1250 cm^{-1} for stretching vibrations of the S=O functional group and at 825 cm^{-1} for the C−O−S functional group. Moreover, the polysaccharide glycosidic bond stretching vibration was observed at 1220 cm^{-1}.

3.3. Hemocompatibility. Functionalized coatings were prepared with the intention of studying the hemocompatibility of potential biodegradable metallic implants with modified surfaces. Material-induced hemolysis (Figure 4) was studied, along with platelet adhesion (Figure 5).
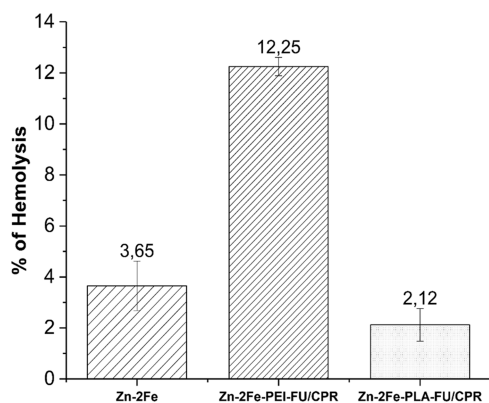

Figure 4. Hemolysis ratio of Zn-2Fe, Zn-2Fe-PEI-FU/CPR, and Zn-2Fe-PLA/CPR samples.

A significant difference was observed between the performance of the PEI and PLA coatings. While the hemolysis of PEI-coated material was as high as 12%, PLA-coated samples showed a six times lower hemolysis ratio (∼2%). The value obtained for the PLA-coated samples was lower than that of pure Zn-2Fe reference indicating its positive effect on hemolysis, which was also reported before.[23] Both pure Zn−Fe and Zn-2Fe-PLA-FU/CPR exhibited a hemolysis rate under 5%, which classifies them as nonhemolytic.

The second parameter monitored for the evaluation of hemocompatibility was the extent of adhesion of blood platelets to the surface of samples immersed in PRP for 1 h. Representative SEM micrographs are depicted in Figure 5. While minimal to no platelets were observed on the surface of pure Zn-2Fe samples (Figure 5a,d), mostly round-shaped platelets with very rare signs of aggregation were found on both coated samples at comparable amounts (Figure 5 b,c,e,f).

3.4. Antibiotic Determination and Release. UV−vis spectroscopy was employed to determine the amount of antibiotic in the polymer coatings. While ∼0.56 mg of CPR was found to be loaded into the PEI coating, only ∼0.31 mg of CPR was present in the PLA coating suggesting a higher capacity of the PEI to be doped with ciprofloxacin when

compared with PLA. The loading efficiency for the PEI coating was 94% while it was only 52% for the PLA.

After the determination of the total amount of CPR in the polymer, its release from the coating was studied (Figure 6). However, only small amounts of the drugs were released after 24−72 h; therefore, another suitable method except for UV−vis spectroscopy needed to be selected for the analysis. Electrochemical methods represent an ideal method for fast, accurate, and simple antibiotic determination. To determine the analytical characteristics of NiNPs/SPCE toward CPR determination, cyclic voltammetry was used. Figure 6e shows the cyclic voltammograms of PBS as a background electrolyte and various concentrations of CPR in PBS (50−500 μM) on NiNPs/SPCE. The peak current corresponding to CPR oxidation on NiNPs/SPCE (E = 0.91 V) increases linearly with increasing antibiotic concentration. These results were fitted by a linear function (Figure 6f) to obtain a correlation coefficient (R^2 = 0.99) for characterizing linearity of the given dependency and the calculation of the sensing characteristics. Based on the obtained results, NiNPs/SPCE displays promising sensing properties for the determination of CPR following a wide linear range from 50 to 500 μM, a high sensitivity of 4.02 mA/μM, and a low LOD of 33.7 μM.

Thereafter, unknown concentrations of CPR released from Zn-2Fe-PEI-FU/CPR and Zn-2Fe-PLA-FU/CPR after 24, 48, and 72 h were determined. Figure 6 shows the cyclic voltammograms of background electrolyte and PBS after 24, 48, and 72 h of CPR release from Zn-2Fe-PEI-FU/CPR (Figure 6a,b) and Zn-2Fe-PLA-FU/CPR (Figure 6c,d). As can be seen in both modifications, the current response increased with the increasing CPR release time. Nevertheless, the peak current corresponding to the oxidation of CPR at NiNPs/SPCE was observed only in the release of CPR from Zn-2Fe-PLA-FU/CPR (Figure 6c,d) when the peak current increases linearly (R^2 = 0.98) with a release time of CPR suggesting controlled gradual release from the PLA. In the case of the PEI, its dissolution may have contributed to this current increase. The concentration of the released CPR from the PLA was calculated based on the calibration curve equation obtained experimentally from the determination of various CIP concentrations (Figure 6e) as 0.17, 0.2, and 0.22 mg for 24, 48, and 72 h, respectively (Figure 6g). However, in the case of PEI modification, no oxidation peak of CPR at potential E = 0.91 V was observed after the studied period, which may be associated with the strongest antibiotic−polymer bond described before.

4. DISCUSSION

A cost-effective, simple, and flexible method of powder metallurgy was used for metallic substrate preparation. The resulting composition, microstructure, and surface morphology of a sintered sample can vary depending on the initial powder characteristics (e.g., grain size and distribution, chemical nature), the sintering conditions (e.g., temperature, atmosphere), and postprocessing steps. The sintering process started with heating the compressed green compact to a high temperature, yet lower than the melting point, which still allows the diffusion of atoms of adjacent metallic particles to form a solid bimetallic material, but does not induce the creation of intermetallic phases. Reduction in the formation of hardly soluble Zn−Fe intermetallic phases, whose presence was observed earlier when a higher temperature was used (350
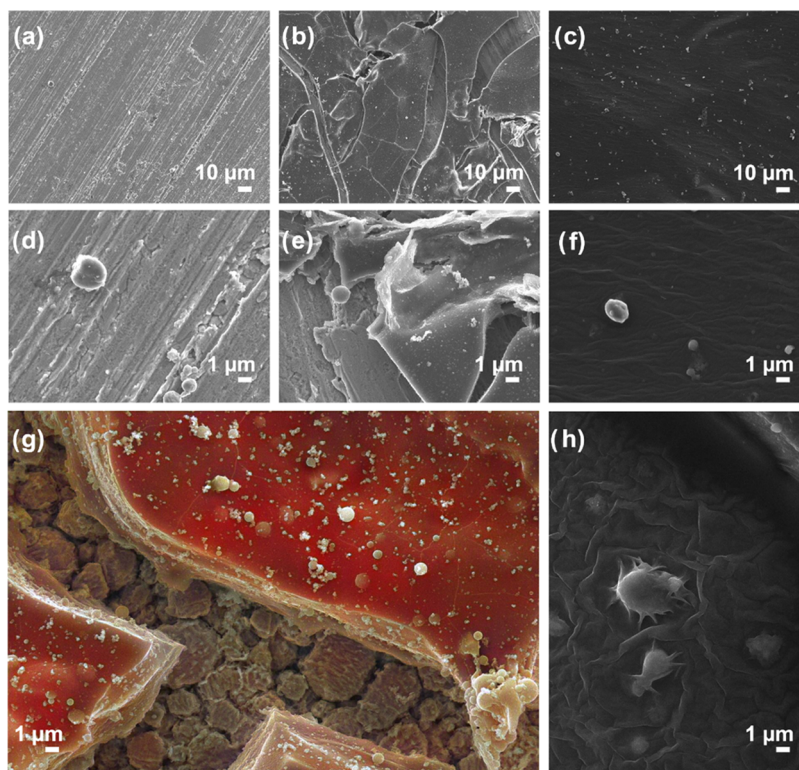
Figure 5. Platelet adhesion on (a, d) Zn-2Fe; (b, e) Zn-2Fe-PEI-FU/CPR; and (c, f) Zn-2Fe-PLA-FU/CPR. (g) Colorized detail of platelet adhesion on Zn-2Fe-PEI-FU/CPR. (h) Detail of platelet adhered on Zn-2Fe-PLA-FU/CPR.

°C),[23] may be beneficial since the prepared material is expected to be fully degraded *in vivo*.

The samples were polished after sintering, and their hydrophilicity/hydrophobicity was studied. In general, a water contact angle greater than 90° is considered high (at levels ≥150° as superhydrophobic), indicating that the surface is hydrophobic or water repulsive. A superhydrophobic can prevent bacterial adhesion and biofilm formation, making it suitable for implantable medical devices.[57] However, highly hydrophobic surfaces may also impede cell adhesion and proliferation at the same time.[58] The calculated surface tension for our Zn-2Fe sample of ~20 mN·m^{-1} can be considered relatively low for a metallic surface. Surfaces with low surface tension may exhibit impaired adhesion properties, as weak cohesive forces can limit the ability to form strong intermolecular bonds with other materials. Therefore, the RF air plasma was further used to activate a metallic sample surface before the first and second coating applications.

PEI and PLA polymeric coatings were successfully deposited on the metallic surface by dip-coating. While the PLA layer was homogeneous and smooth even after the application of the second (FU/CPR) coating, the PEI layer exhibited extensive cracking. Even though these cracks have disturbed the layer, several cases, including our previous work, were reported where these can play the role of a canal for better electrolyte penetration and therefore play a role in corrosion process dynamics.[46,59] Effective incorporation of dopants (FU/CPR) into both polymers was confirmed by the FT-IR method. The higher loading efficiency (almost double) was observed for the PEI owing to its conductive character and therefore more efficient bonding with dopants rich in functional groups. The whole group of conductive polymers is arising nowadays in various applications, not excluding tissue engineering, due to

the electrically excitable nature of body tissues, thus the positive influence of electrical stimulation on regeneration processes.[60]

Even though PEI showed favorable properties related to the loading capacity, biological performance (e.g., hemocompatibility) is still of key importance. Nonacceptable hemolysis (12%) was observed in a case of PEI use. Hemolysis, the breakdown or rupture of erythrocytes, leads to leakage of their contents into the surrounding body fluid. This can occur as a result of exposure to certain molecules. PEI is a cationic polymer that can interact with the negatively charged surfaces of red blood cells, leading to their lysis. PEI is also known to disrupt the cell membrane and increase its permeability,[61] which can lead to the release of hemoglobin and other cellular contents into the bloodstream. In addition, PEI can induce aggregation of erythrocytes, which can also contribute to hemolysis.[62] The exact mechanism by which PEI induces hemolysis is not fully understood and may depend on its molecular weight, charge density, and concentration in the coating. Ten wt % PEI coating, even when treated with fucoidan, did show an inadequate hemolysis ratio, unlike the 2.5 wt % PLA coating, leading to decreased hemolysis when compared with the uncoated metal. Owing to its nature, PLA inhibited the degradation of the metal matrix itself, which could also contribute to reducing the effect of hemolysis. Also, a significantly lower concentration of PLA was used when compared with PEI. According to previous studies, PLA concentration is a key factor determining its hemolytic properties.[63] The smooth coating in the case of PLA, opposite to the cracked PEI layer, minimizes areas where blood can stagnate or become trapped, which may also lead to more prevalent hemolysis.
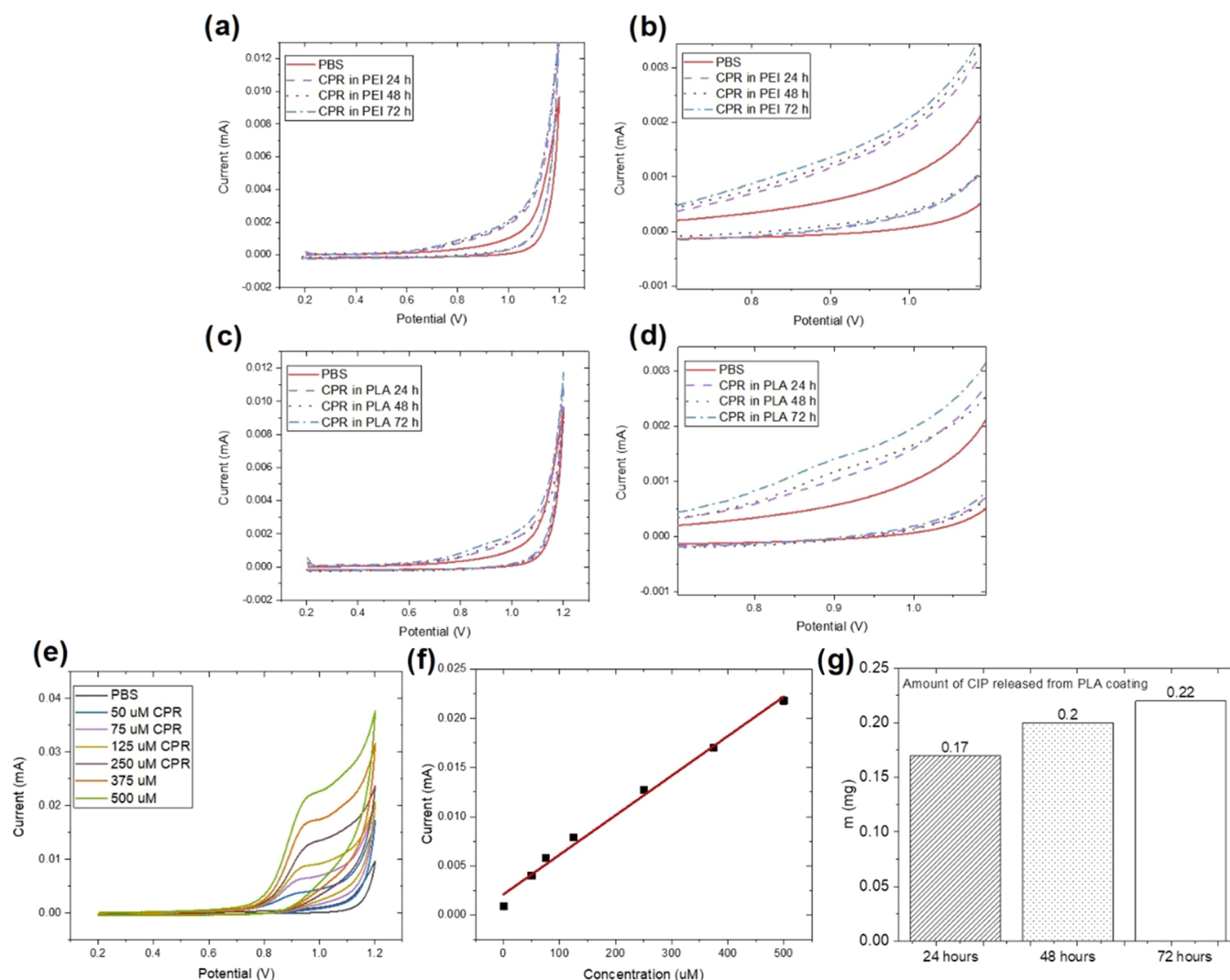
Figure 6. (a) Cyclic voltammograms of background electrolyte and unknown concentrations of CPR released after 24, 48, and 72 h from Zn-2Fe-PEI-FU/CPR on NiNPs/SPCE at a scan rate of 100 mV/s with detail (b). (c) Cyclic voltammograms of background electrolyte and unknown concentrations of CPR released after 24, 48, and 72 h from Zn-2Fe-PLA-FU/CPR on NiNPs/SPCE at a scan rate of 100 mV/s with the detail (d). (e) Cyclic voltammograms of different CPR concentrations on NiNPs/SPCE at a scan rate of 100 mV/s. (e) The dependence of the maximum peak current on the CPR concentration, as fitted by a linear function. (f) Calibration curve: dependence of current vs concentration of CIP. (g) Ciprofloxacin released from PLA coating over 24, 48, and 72 h.

Along the hemolysis, platelet adhesion was observed. No to minimal platelet adhesion was observed for bare metal, while a slightly increased amount of mostly inactivated platelets was observed for coated samples. Fucoidans have been shown to inhibit the activation of platelets, which play a key role in clot formation. Platelets can aggregate to form a thrombus upon their activation while fucoidans inhibit platelet activation by blocking the binding of platelets to fibrinogen, a protein that is involved in a clot formation process.[64] Factors that also contribute to platelet adhesion are the surface energy of the material and the presence of functional groups that can interact with platelet receptors, leading to an increased adhesion. Polymers have typically lower surface energies than metals, leading to a higher tendency of platelet adhesion, while these low surface energies can also make polymers more susceptible to platelet adhesion promoting protein adsorption, which may explain the more prevalent occurrence of platelets on the coated samples.

Besides fucoidan, surfaces were also modified by the addition of the antibiotic component ciprofloxacin. The chemical properties (side chains) of the polymers, the nature and mechanism of the drug–polymer interactions, and the preparation route selected to fabricate the drug-loaded polymer coating may all affect the amount of the drug that will be bonded into the polymer. We assume that PEI, due to its polycationic nature, can form electrostatic interactions with the anionic carboxylic acid groups in ciprofloxacin, which can lead to a higher drug loading and binding efficiency. On the other hand, PLA is a hydrophobic polymer with a lower surface charge density that may lead to limited bonding possibilities but, on the other hand, to the more likely antibiotic release.

To get the relevant results of the drug (CPR) release, a suitable electrochemical sensor for the determination of CPR in PBS with a low limit of detection (LOD), high sensitivity, wide linear range, and high specificity must be chosen. Based on the obtained results, SPCE modified with NiNPs (NiNPs/SPCE) can be considered to be a potential electrochemical

sensor for CPR determination. Compared with other currently used methods for CPR determination like high-performance liquid chromatography (HPLC)[65,66] and UV−vis spectroscopy,[67] when LOD was calculated as ∼300 μM and the sensitivity of mentioned methods was determined as ∼1.60 mA/μM,[65,66,68] using electrochemical methods for CPR determination leads to rapid LOD decrease and stability improvement. Moreover, enzymatic sensors for CPR have been developed and tested for CPR determination.[69] The huge disadvantage of these sensors is their high price, low stability, and narrow linear range arising from the enzyme used.[69] Another study focused on the use of boron-doped diamond electrodes,[70] which represent a more financially demanding sensor compared with NiNPs/SPCE described in this work. Slow, gradual release of CPR was detected for PLA modification; however, no CPR was released over 72 h in the case of PEI, associated with the stronger bonding discussed before. Therefore, longer times for the drug release from the PEI coating need to be further examined along with the antibacterial activity tests' performance.

5. CONCLUSIONS

An ideal degradable biomaterial must provide sufficient mechanical support, but at the same time show low toxicity and high hemocompatibility and, ideally, also bring added therapeutic value, e.g., in the form of targeted drug release. The main goal of this study was to prepare a material that addresses the problems of insufficient mechanical properties of pure zinc and excessive release of potentially toxic zinc ions and is enriched with anticoagulant and antibacterial agents at the same time. Zinc−iron alloy was successfully prepared by the powder metallurgy method, which led to the creation of a zinc-based material with nonhomogeneously distributed iron particles, which can enhance the insufficient mechanical properties of pure zinc. Polymer coatings comprised of PEI or PLA were successfully deposited by the dip-coating method with a concentration of 10 wt % and 2.5% for PEI and PLA, respectively. These polymer layers were also modified with ciprofloxacin and fucoidan for the enhancement of anticoagulant and antimicrobial activity. Coating with the polymer layer may also help with potential zinc toxicity related to excessive ion release by slowing down the corrosion rate. The EDX and FT-IR analyses confirmed the successful deposition of both FU and CPR as second coatings. Different surface morphology was observed for PEI- and PLA-coated samples due to the intensive cracking that occurred in the case of PEI and was not observed in the case of PLA. The CPR loading in the polymer was almost two times higher for PEI when compared with PLA. Blood tests showed a sufficiently low hemolysis ratio when PLA or uncoated sample was used while the PEI-coated samples showed a nonacceptable hemolysis rate of over 12%, which disqualifies PEI at this concentration (10 wt %) from further use in blood-contacting devices. Moreover, gradual release of ciprofloxacin from PLA was observed (0.5, 0.59, and 0.65 mM for 24, 48, and 72 h, respectively) while no drug release after 72 h was spotted in the case of PEI. These findings suggest the use of the PLA platform as a promising coating material for biodegradable materials that are intended to be used in contact with blood with the potential to become sufficient drug carriers as well. Therefore, the PLA-based coating system was selected for future use and antimicrobial activity, long-term degradation, and cell tests.

■ ASSOCIATED CONTENT

Ⓢ Supporting Information

The Supporting Information is available free of charge at https://pubs.acs.org/doi/10.1021/acsomega.3c06048.

> Contact angle measurements and hemocompatibility tests experimental methods (PDF)

■ AUTHOR INFORMATION

Corresponding Author

Ivana Šišoláková − *Department of Physical Chemistry, Faculty of Science, Pavol Jozef Šafárik University in Košice, 041 54 Košice, Slovakia; Centre of Polymer Systems, University Institute, Tomas Bata University in Zlín, 760 01 Zlín, Czech Republic;* ⓞ orcid.org/0000-0003-1940-7786; Email: ivana.sisolakova@upjs.sk

Authors

Radka Gorejová − *Department of Physical Chemistry, Faculty of Science, Pavol Jozef Šafárik University in Košice, 041 54 Košice, Slovakia; Centre of Polymer Systems, University Institute, Tomas Bata University in Zlín, 760 01 Zlín, Czech Republic*

Kadir Ozaltin − *Centre of Polymer Systems, University Institute, Tomas Bata University in Zlín, 760 01 Zlín, Czech Republic;* ⓞ orcid.org/0000-0002-7619-5321

Miriam Kupková − *Institute of Materials Research, Slovak Academy of Sciences, 040 01 Košice, Slovakia*

Petr Sáha − *Centre of Polymer Systems, University Institute, Tomas Bata University in Zlín, 760 01 Zlín, Czech Republic*

Renáta Oriňaková − *Department of Physical Chemistry, Faculty of Science, Pavol Jozef Šafárik University in Košice, 041 54 Košice, Slovakia; Centre of Polymer Systems, University Institute, Tomas Bata University in Zlín, 760 01 Zlín, Czech Republic;* ⓞ orcid.org/0000-0001-8103-2634

Complete contact information is available at:
https://pubs.acs.org/10.1021/acsomega.3c06048

Author Contributions

The manuscript was written through the contributions of all authors. All authors have given approval to the final version of the manuscript.

Notes

The authors declare no competing financial interest.

■ ABBREVIATIONS

AFM –atomic force microscopy; BM –biodegradable materials; CPR –ciprofloxacin; FT-IR –Fourier transform infrared spectroscopy; FU –fucoidan; LOD –limit of detection; NiNPs

–Nickel nanoparticles; PEI –polyethylenimine; PLA –poly lactic acid; SEM –scanning electron microscopy; SPCEs –screen-printed carbon electrodes

■ REFERENCES

(1) Hudecki, A.; Kiryczyński, G.; Łos, M. J. Biomaterials, Definition, Overview. *Stem Cells Biomater. Regener. Med.* **2019**, *ii*, 85–98.

(2) Ratner, B. D.; Bryant, S. J. Biomaterials: Where We Have Been and Where We Are Going. *Annu. Rev. Biomed. Eng.* **2004**, *6* (1), 41–75.

(3) Kuhn, L. T. Biomaterials. In *Introduction to Biomedical Engineering*, Second ed.; Elsevier, 2005; pp 255–312.

(4) Thouas, G. A.; Chen, Q. Metallic Implant Biomaterials. *Mater. Sci. Eng., R* **2015**, *87*, 1–57.

(5) Biswal, T.; BadJena, S. K.; Pradhan, D. Sustainable Biomaterials and Their Applications: A Short Review. *Mater. Today Proc.* **2020**, *30*, 274–282.

(6) Radenkovic, G.; Petkovic, D. Metallic Biomaterials. In *Biomaterials in Clinical Practice*; Springer: Cham, 2017; p 183.

(7) Todros, S.; Todesco, M.; Bagno, A. Biomaterials and Their Biomedical Applications: From Replacement to Regeneration. *Processes* **2021**, *9* (11), 1949.

(8) Yun, Y.; Dong, Z.; Lee, N.; Liu, Y.; Xue, D.; Guo, X.; Kuhlmann, J.; Doepke, A.; Halsall, H. B.; Heineman, W.; et al. Revolutionizing Biodegradable Metals. *Mater. Today* **2009**, *12* (10), 22–32.

(9) Li, H.; Zheng, Y.; Qin, L. Progress of Biodegradable Metals. *Prog. Nat. Sci. Mater. Int.* **2014**, *24* (5), 414–422, DOI: 10.1016/j.pnsc.2014.08.014.

(10) Wei, S.; Ma, J. X.; Xu, L.; Gu, X. S.; Ma, X. L. Biodegradable Materials for Bone Defect Repair. *Mil. Med. Res.* **2020**, *7* (1), No. 54.

(11) Godavitarne, C.; Robertson, A.; Peters, J.; Rogers, B. Biodegradable Materials. *Orthop. Trauma* **2017**, *31* (5), 316–320.

(12) Yang, Y.; He, C.; Dianyu, E.; Yang, W.; Qi, F.; Xie, D.; Shen, L.; Peng, S.; Shuai, C. Mg Bone Implant: Features, Developments and Perspectives. *Mater. Des.* **2020**, *185*, No. 108259.

(13) Yusop, A. H.; Bakir, A. A.; Shaharom, N. A.; Abdul Kadir, M. R.; Hermawan, H. Porous Biodegradable Metals for Hard Tissue Scaffolds: A Review. *Int. J. Biomater.* **2012**, *2012*, 1–10.

(14) Hermawan, H. Updates on the Research and Development of Absorbable Metals for Biomedical Applications. *Prog. Biomater.* **2018**, *7*, 93–110.

(15) Pospíšilová, I.; Vojtěch, D. Zinc Alloys for Biodegradable Medical Implants. *Mater. Sci. Forum* **2014**, *782* (April 2014), 457–460.

(16) Zhang, J.; Shang, Z.; Jiang, Y.; Zhang, K.; Li, X.; Ma, M.; Li, Y.; Ma, B. Biodegradable Metals for Bone Fracture Repair in Animal Models: A Systematic Review. *Regener. Biomater.* **2021**, *8* (1), No. rbaa047.

(17) Shishir, R.; Lokeshkumar, E.; Manojkumar, P.; Nasiruddin, U.; Premchand, C.; Ponnilavan, V.; Rama Krishna, L.; R, N. Development of Biocompatible and Corrosion-Resistant Plasma Electrolytic Oxidation Coating over Zinc for Orthopedic Implant Applications. *Surf. Coat. Technol.* **2022**, *450*, No. 128990.

(18) Levy, G. K.; Goldman, J.; Aghion, E. The Prospects of Zinc as a Structural Material for Biodegradable Implants—a Review Paper. *Metals* **2017**, *7* (10), No. 402.

(19) Mulinti, P.; Brooks, J. E.; Lervick, B.; Pullan, J. E.; Brooks, A. E. Strategies to Improve the Hemocompatibility of Biodegradable Biomaterials. In *Hemocompatibility of Biomaterials for Clinical Applications: Blood-Biomaterials Interactions*; Elsevier Ltd, 2018; pp 253–278.

(20) Bagha, P. S.; Khakbiz, M.; Sheibani, S.; Ebrahimi-Barough, S.; Hermawan, H. In Vitro Degradation, Hemocompatibility, and Cytocompatibility of Nanostructured Absorbable Fe-Mn-Ag Alloys for Biomedical Application. *ACS Biomater. Sci. Eng.* **2020**, *6* (4), 2094–2106.

(21) Yin, Y. X.; Zhou, C.; Shi, Y. P.; Shi, Z. Z.; Lu, T. H.; Hao, Y.; Liu, C. H.; Wang, X.; Zhang, H. J.; Wang, L. N. Hemocompatibility of Biodegradable Zn-0.8 wt% (Cu, Mn, Li) Alloys. *Mater. Sci. Eng., C* **2019**, *104*, No. 109896.

(22) Nie, F. L.; Zheng, Y. F.; Wei, S. C.; Hu, C.; Yang, G. In Vitro Corrosion, Cytotoxicity and Hemocompatibility of Bulk Nanocrystalline Pure Iron. *Biomed. Mater.* **2010**, *5* (6), No. 065015, DOI: 10.1088/1748-6041/5/6/065015.

(23) Králová, Z. O.; Gorejová, R.; Oriňaková, R.; Petráková, M.; Oriňak, A.; Kupková, M.; Hrubovčáková, M.; Sopčák, T.; Baláž, M.; Maskalová, I.; et al. Biodegradable Zinc-Iron Alloys: Complex Study of Corrosion Behavior, Mechanical Properties and Hemocompatibility. *Prog. Nat. Sci. Mater. Int.* **2021**, *31* (2), 279–287.

(24) Shen, C.; Liu, X.; Fan, B.; Lan, P.; Zhou, F.; Li, X.; Wang, H.; Xiao, X.; Li, L.; Zhao, S.; et al. Mechanical Properties,: In Vitro Degradation Behavior, Hemocompatibility and Cytotoxicity Evaluation of Zn-1.2Mg Alloy for Biodegradable Implants. *RSC Adv.* **2016**, *6* (89), 86410–86419.

(25) Cheng, J.; Huang, T.; Zheng, Y. F. Microstructure, Mechanical Property, Biodegradation Behavior, and Biocompatibility of Biodegradable Fe-Fe2O3 Composites. *J. Biomed. Mater. Res., Part A* **2014**, *102*, 2277.

(26) Luo, R.; Tang, L.; Zhong, S.; Yang, Z.; Wang, J.; Weng, Y.; Tu, Q.; Jiang, C.; Huang, N. In Vitro Investigation of Enhanced Hemocompatibility and Endothelial Cell Proliferation Associated with Quinone-Rich Polydopamine Coating. *ACS Appl. Mater. Interfaces* **2013**, *5* (5), 1704–1714.

(27) Gao, Q.; Li, X.; Yu, W.; Jia, F.; Yao, T.; Jin, Q.; Ji, J. Fabrication of Mixed-Charge Polypeptide Coating for Enhanced Hemocompatibility and Anti-Infective Effect. *ACS Appl. Mater. Interfaces* **2020**, *12* (2), 2999–3010.

(28) Johnbosco, C.; Zschoche, S.; Nitschke, M.; Hahn, D.; Werner, C.; Maitz, M. F. Bioresponsive StarPEG-Heparin Hydrogel Coatings on Vascular Stents for Enhanced Hemocompatibility. *Mater. Sci. Eng., C* **2021**, *128*, No. 112268.

(29) Li, J.; Zhang, K.; Ma, W.; Wu, F.; Yang, P.; He, Z.; Huang, N. Investigation of Enhanced Hemocompatibility and Tissue Compatibility Associated with Multi-Functional Coating Based on Hyaluronic Acid and Type IV Collagen. *Regener. Biomater.* **2016**, *3* (3), 149–157.

(30) Li, P.; Li, L.; Wang, W.; Jin, W.; Liu, X.; Yeung, K. W. K.; Chu, P. K. Enhanced Corrosion Resistance and Hemocompatibility of Biomedical NiTi Alloy by Atmospheric-Pressure Plasma Polymerized Fluorine-Rich Coating. *Appl. Surf. Sci.* **2014**, *297*, 109–115.

(31) Shi, Z. Z.; Gao, X. X.; Zhang, H. J.; Liu, X. F.; Li, H. Y.; Zhou, C.; Yin, Y. X.; Wang, L. N. Design Biodegradable Zn Alloys: Second Phases and Their Significant Influences on Alloy Properties. *Bioact. Mater.* **2020**, *5* (2), 210–218.

(32) Liu, X.; Sun, J.; Zhou, F.; Yang, Y.; Chang, R.; Qiu, K.; Pu, Z.; Li, L.; Zheng, Y. Micro-Alloying with Mn in Zn–Mg Alloy for Future Biodegradable Metals Application. *Mater. Des.* **2016**, *94*, 95–104.

(33) Ali, M.; Elsherif, M.; Salih, A. E.; Ul-Hamid, A.; Hussein, M. A.; Park, S.; Yetisen, A. K.; Butt, H. Surface Modification and Cytotoxicity of Mg-Based Bio-Alloys: An Overview of Recent Advances. *J. Alloys Compd.* **2020**, *825*, No. 154140.

(34) Smith, J. R.; Lamprou, D. A. Polymer Coatings for Biomedical Applications: A Review. *Trans. Inst. Met. Finish.* **2014**, *92* (1), 9–19.

(35) Zhu, Y.; Liu, W.; Ngai, T. Polymer Coatings on Magnesium-Based Implants for Orthopedic Applications. *J. Polym. Sci.* **2022**, *60* (1), 32–51.

(36) Szaraniec, B.; Pielichowska, K.; Pac, E.; Menaszek, E. Multifunctional Polymer Coatings for Titanium Implants. *Mater. Sci. Eng., C* **2018**, *93*, 950–957.

(37) Li, L. Y.; Cui, L. Y.; Zeng, R. C.; Li, S. Q.; Chen, X. B.; Zheng, Y.; Kannan, M. B. Advances in Functionalized Polymer Coatings on Biodegradable Magnesium Alloys − A Review. *Acta Biomater.* **2018**, *79*, 23–36.

(38) Priyadarshini, B.; Chetan, M. R.; Vijayalakshmi, U. Bioactive Coating as a Surface Modification Technique for Biocompatible

Metallic Implants: A Review. *J. Asian Ceram. Soc.* **2019**, 7 (4), 397−406.

(39) Zeng, R. C.; Cui, L. Y.; Jiang, K.; Liu, R.; Zhao, B. D.; Zheng, Y. F. In Vitro Corrosion and Cytocompatibility of a Microarc Oxidation Coating and Poly(l -Lactic Acid) Composite Coating on Mg-1Li-1Ca Alloy for Orthopedic Implants. *ACS Appl. Mater. Interfaces* **2016**, 8 (15), 10014−10028.

(40) Bakhsheshi-Rad, H. R.; Akbari, M.; Ismail, A. F.; Aziz, M.; Hadisi, Z.; Pagan, E.; Daroonparvar, M.; Chen, X. Coating Biodegradable Magnesium Alloys with Electrospun Poly-L-Lactic Acid-Åkermanite-Doxycycline Nanofibers for Enhanced Biocompatibility, Antibacterial Activity, and Corrosion Resistance. *Surf. Coat. Technol.* **2019**, 377, No. 124898.

(41) Santoro, M.; Shah, S. R.; Walker, J. L.; Mikos, A. G. Poly(Lactic Acid) Nanofibrous Scaffolds for Tissue Engineering. *Adv. Drug Delivery Rev.* **2016**, 107, 206−212.

(42) Yao, X.; Zhou, N.; Wan, L.; Su, X.; Sun, Z.; Mizuguchi, H.; Yoshioka, Y.; Nakagawa, S.; Zhao, R. C.; Gao, J. Q. Polyethyleneimine-Coating Enhances Adenoviral Transduction of Mesenchymal Stem Cells. *Biochem. Biophys. Res. Commun.* **2014**, 447 (3), 383−387.

(43) Xia, T.; Kovochich, M.; Liong, M.; Meng, H.; Kabehie, S.; George, S.; Zink, J. I.; Nel, A. E. Polyethyleneimine Coating Enhances the Cellular Uptake of Mesoporous Silica Nanoparticles and Allows Safe Delivery of SiRNA and DNA Constructs. *ACS Nano* **2009**, 3 (10), 3273−3286.

(44) Thomas, T. J.; Tajmir-Riahi, H. A.; Pillai, C. K. S. Biodegradable Polymers for Gene Delivery. *Molecules* **2019**, 24 (20), 3744.

(45) Bastarrachea, L. J.; Goddard, J. M. Self-Healing Antimicrobial Polymer Coating with Efficacy in the Presence of Organic Matter. *Appl. Surf. Sci.* **2016**, 378, 479−488.

(46) Gorejová, R.; Oriňaková, R.; Macko, J.; Oriňak, A.; Kupková, M.; Hrubovčáková, M.; Džupon, M.; Sopčák, T.; Ševc, J.; Maskaľová, I.; Džunda, R. Electrochemical Behavior, Biocompatibility and Mechanical Performance of Biodegradable Iron with PEI Coating. *J. Biomed. Mater. Res., Part A* **2022**, 110 (3), 659−671.

(47) Pritchard, E. M.; Valentin, T.; Panilaitis, B.; Omenetto, F.; Kaplan, D. L. Antibiotic-Releasing Silk Biomaterials for Infection Prevention and Treatment. *Adv. Funct. Mater.* **2013**, 23 (7), 854−861.

(48) Ahmed, W.; Zhai, Z.; Gao, C. Adaptive Antibacterial Biomaterial Surfaces and Their Applications. In *Materials Today Bio.*; Elsevier B.V., March 1, 2019.

(49) Gottenbos, B.; Busscher, H. J.; Van Der Mei, H. C.; Nieuwenhuis, P. Pathogenesis and Prevention of Biomaterial Centered Infections. *J. Mater. Sci. Mater. Med.* **2002**, 13, 717−722.

(50) Mishra, N.; Jain, P. A Comprehensive Review on Transdermal Patch of Ciprofloxacin Hydrochloride. *Int. J. Adv. Pharm. Med. Bioallied Sci.* **2022**, 10 (2), 82−87, DOI: 10.5281/zenodo.7047439.

(51) Esrafilzadeh, D.; Razal, J. M.; Moulton, S. E.; Stewart, E. M.; Wallace, G. G. Multifunctional Conducting Fibres with Electrically Controlled Release of Ciprofloxacin. *J. Controlled Release* **2013**, 169 (3), 313−320.

(52) Kyzioł, A.; Michna, J.; Moreno, I.; Gamez, E.; Irusta, S. Preparation and Characterization of Electrospun Alginate Nanofibers Loaded with Ciprofloxacin Hydrochloride. *Eur. Polym. J.* **2017**, 96, 350−360.

(53) Krukiewicz, K.; Gniazdowska, B.; Jarosz, T.; Herman, A. P.; Boncel, S.; Turczyn, R. Effect of Immobilization and Release of Ciprofloxacin and Quercetin on Electrochemical Properties of Poly(3,4-Ethylenedioxypyrrole) Matrix. *Synth. Met.* **2019**, 249, 52−62.

(54) Irhimeh, M. R.; Fitton, J. H.; Lowenthal, R. M. Pilot Clinical Study to Evaluate the Anticoagulant Activity of Fucoidan. *Blood Coagulation Fibrinolysis* **2009**, 20 (7), 607−610.

(55) Cumashi, A.; Ushakova, N. A.; Preobrazhenskaya, M. E.; D'Incecco, A.; Piccoli, A.; Totani, L.; Tinari, N.; Morozevich, G. E.; Berman, A. E.; Bilan, M. I.; et al. A Comparative Study of the Anti-Inflammatory, Anticoagulant, Antiangiogenic, and Antiadhesive Activities of Nine Different Fucoidans from Brown Seaweeds. *Glycobiology* **2007**, 17 (5), 541−552.

(56) Husni, A.; Izmi, N.; Ayunani, F. Z.; Kartini, A.; Husnayain, N.; Isnansetyo, A. Characteristics and Antioxidant Activity of Fucoidan from Sargassum Hystrix: Effect of Extraction Method. *Int. J. Food Sci.* **2022**, 2022, No. 3689724.

(57) Yuan, Y.; Hays, M. P.; Hardwidge, P. R.; Kim, J. Surface Characteristics Influencing Bacterial Adhesion to Polymeric Substrates. *RSC Adv.* **2017**, 7 (23), 14254−14261.

(58) Al-Azzam, N.; Alazzam, A. Micropatterning of Cells via Adjusting Surface Wettability Using Plasma Treatment and Graphene Oxide Deposition. *PLoS One* **2022**, 17 (6), No. e0269914.

(59) Yusop, A. H. M.; Daud, N. M.; Nur, H.; Kadir, M. R. A.; Hermawan, H.; Hakim, A.; Yusop, M.; Daud, N. M.; Nur, H.; Rafiq, M.; et al. Controlling the Degradation Kinetics of Porous Iron by Poly(Lactic-Co-Glycolic Acid) Infiltration for Use as Temporary Medical Implants. *Sci. Rep.* **2015**, 5, No. 11194.

(60) Dixon, D. T.; Gomillion, C. T. 3D-Printed Conductive Polymeric Scaffolds with Direct Current Electrical Stimulation for Enhanced Bone Regeneration. *J. Biomed. Mater. Res., Part B* **2023**, 111, 1351−1364, DOI: 10.1002/jbm.b.35239.

(61) Ira, Y. M.; Krishnamoorthy, G. DNA Vector Polyethyleneimine Affects Cell PH and Membrane Potential: A Time-Resolved Fluorescence Microscopy Study. *J. Fluoresc.* **2003**, 13 (4), 339−347.

(62) Zhong, D.; Jiao, Y.; Zhang, Y.; Zhang, W.; Li, N.; Zuo, Q.; Wang, Q.; Xue, W.; Liu, Z. Effects of the Gene Carrier Polyethyleneimines on Structure and Function of Blood Components. *Biomaterials* **2013**, 34 (1), 294−305.

(63) Libi, S.; Calenic, B.; Astete, C. E.; Kumar, C.; Sabliov, C. M. Investigation on Hemolytic Effect of Poly(Lactic Co-Glycolic) Acid Nanoparticles Synthesized Using Continuous Flow and Batch Processes. *Nanotechnol. Rev.* **2017**, 6 (2), 209−220.

(64) Diirig', J.; Bruhn2, T.; Zurbornl, K.-H.; Gutensohn3, K.; Bruhn', H. D.; Béress, L.; Durig, J. Anticoagulant fucoidan fractions from Fucus vesiculosus induce platelet activation in vitro. *Thromb Res.* **1997**, 85 (6), 479−491, DOI: 10.1016/s0049-3848(97)00037-6.

(65) Imre, S.; Dogaru, M. T.; Vari, C. E.; Muntean, T.; Kelemen, L. Validation of an HPLC Method for the Determination of Ciprofloxacin in Human Plasma. *J. Pharm. Biomed. Anal.* **2003**, 33 (1), 125−130.

(66) Vybíralová, Z.; Nobilis, M.; Zoulova, J.; Květina, J.; Petr, P. High-Performance Liquid Chromatographic Determination of Ciprofloxacin in Plasma Samples. *J. Pharm. Biomed. Anal.* **2005**, 37, 851−858, DOI: 10.1016/j.jpba.2004.09.034.

(67) Vella, J.; Busuttil, F.; Bartolo, N. S.; Sammut, C.; Ferrito, V.; Serracino-Inglott, A.; Azzopardi, L. M.; LaFerla, G. A Simple HPLC-UV Method for the Determination of Ciprofloxacin in Human Plasma. *J. Chromatogr. B: Anal. Technol. Biomed. Life Sci.* **2015**, 989, 80−85.

(68) Fratini, L.; Schapoval, E. S. Ciprofloxacin Determination by Visible Light Spectrophotometry Using Iron(III)Nitrate. *Int. J. Pharm.* **1996**, 127 (2), 279−282, DOI: 10.1016/0378-5173(95)04290-3.

(69) Torriero, A. A. J.; Ruiz-Díaz, J. J. J.; Salinas, E.; Marchevsky, E. J.; Sanz, M. I.; Raba, J. Enzymatic Rotating Biosensor for Ciprofloxacin Determination. *Talanta* **2006**, 69 (3), 691−699.

(70) Cinková, K.; Andrejčáková, D.; Švorc, L'. Electrochemical Method for Point-of-Care Determination of Ciprofloxacin Using Boron-Doped Diamond Electrode. *Acta Chim. Slovaca* **2016**, 9 (2), 146−151.